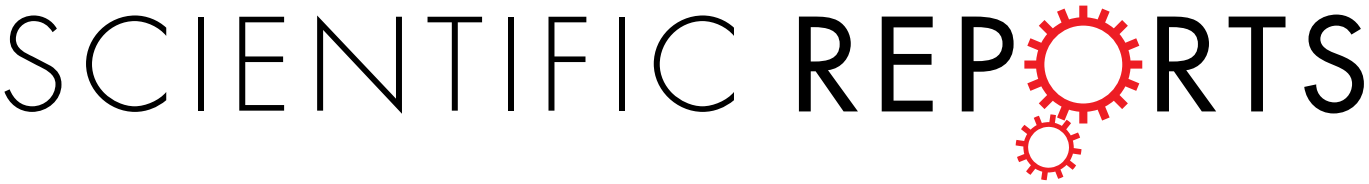

OPEN

Received: 7 July 2017
Accepted: 11 September 2017
Published online: 22 September 2017

Aligned hierarchical Ag/ZnO nano-heterostructure arrays via electrohydrodynamic nanowire template for enhanced gas-sensing properties

Zhouping Yin[1,2], Xiaomei Wang[3], Fazhe Sun[4], Xiaohu Tong[5], Chen Zhu[1,2], Qiying Lv[6], Dong Ye[1,2], Shuai Wang[6], Wei Luo[5] & YongAn Huang[1,2]

Gas sensing performance can be improved significantly by the increase in both the effective gas exposure area and the surface reactivitiy of ZnO nanorods. Here, we propose aligned hierarchical Ag/ZnO nano-heterostructure arrays (h-Ag/ZnO-NAs) via electrohydrodynamic nanowire template, together with a subsequent hydrothermal synthesis and photoreduction reaction. The h-Ag/ZnO-NAs scatter at top for higher specific surface areas with the air, simultaneously contact at root for the electrical conduction. Besides, the ZnO nanorods are uniformly coated with dispersed Ag nanoparticles, resulting in a tremendous enhancement of the surface reactivity. Compared with pure ZnO, such h-Ag/ZnO-NAs exhibit lower electrical resistance and faster responses. Moreover, they demonstrate enhanced NO_2 gas sensing properties. Self-assembly via electrohydrodynamic nanowire template paves a new way for the preparation of high performance gas sensors.

The quantitative detection of noxious gas such as Nitrogen dioxide (NO_2) has been drawn considerable attention. Semiconducting metal oxides, especially ZnO, have been commonly used as the active sensing materials for gas sensors due to their fast response, short response-recovery time, excellent electrical performance, and long term stability[1–3]. Recently, researches have focused on enhancing the gas sensing performance of ZnO nanostructures by using nanostructured materials with ultra-high specific surface areas[4–6], appropriate element doping[7–10], surface decoration with noble metals (Au, Pt, Pd, and Ag)[11–14] nanocomposite[15–17] and construction of heterostructure[18–22]. Among them, the hierarchical nano-heterostructures have attracted great attention due to their rich architectures, extraordinary properties, and novel applications[23,24]. The decoration of nanostructures with noble metal nanoparticles can further enhance multiple gas-sensing performance[25]. A simple way was developed to fix Au on ZnO microrods, and the obtained Au decorated ZnO microrods showed enhanced sensing performance towards ethanol detection[26]. The preparation of Pt modified ZnO nanowires was demonstrated for room temperature ethanol sensing[27]. ZnO nanostructures decorated with Pd were synthesized through self-assemblies, and the obtained hybrid material exhibited a great improvement on sensitivity to H_2S gas[28]. Unfortunately, most ZnO film-like precursor are too dense so that the ZnO nanorods usually exhibit rather compact. The exposure area of the target gas molecules in sensing is too low even if the ZnO nanorods modified with noble metals or oxides. A high exposure area with the gas can be achieved at the case of low-density ZnO nanorods; however, the conductivity is usually below the minimum detection limit.

[1]State Key Laboratory of Digital Manufacturing Equipment and Technology, Huazhong University of Science and Technology, Wuhan, 430074, China. [2]Flexible Electronics Research Center, Huazhong University of Science and Technology, Wuhan, 430074, China. [3]School of Science, Shandong University of Technology, Zibo, 255100, China. [4]Analysis Testing Center, Shandong University of Technology, Zibo, 255100, China. [5]School of Optical and Electronic Information, Huazhong University of Science and Technology, Wuhan, 430074, China. [6]School of Chemistry and Chemical Engineering, Huazhong University of Science and Technology, Wuhan, 430074, China. Zhouping Yin and Xiaomei Wang contributed equally to this work. Correspondence and requests for materials should be addressed to Y.H. (email: yahuang@hust.edu.cn)

It is important to address the paradox between the conductivity of the cluster of ZnO nanostructures and the exposure area with the gas. When ribbon-like precursor are adopted, ZnO nanorods at edges and corners would scatter to enhance the specific area, while the others still keep similar with those grown on film-like precursor. By replacing ribbon-like precursor with nanowire-like one, the specific area of ZnO nanorods will be futher improved as a result of the formation of brush-like hierarchical nanostructures, and the tight contact of nanorods at root is also beneficial to the transfer of electrons. However, the traditional synthesis methods[29], such as traditional ink-jet printing, aerosol-based nanotechnology, physical vapor deposition, chemical vapor deposition and hydrothermal method, are unable to fabricate surface-modified, aligned hierarchical nanostructures.

In view of this, herein, we present a newly-proposed approach to fabricate aligned hierarchical Ag/ZnO nano-heterostructure arrays (Ag/ZnO-NAs) in a digital, large-area and cost-effective manner, through electrohydrodynamic direct-writing polymer nanowire template followed by hydrothermal growth and photoreduction. The Ag/ZnO-NAs combine the advantage of surface modification and hierarchical nano-heterostructures, and this effect tremendously enhance the gas sensing performances. Moreover, the Ag/ZnO-NAs exhibit an excellent selectivity for NO_2 gas sensing. The gas sensing performance of hierarchical ZnO nanorods with various precursor pattern (line-width and gap) and Ag contents (corresponding to Ag+ photoreduction time) has been systematically evaluated and the optimal layout of precursor and photoreduction time have been discovered. The corresponding mechanism has been discussed as well.

Results and Discussion

Figure 1a conceptually depicts the stepwise manufacturing procedure brush-like Ag/ZnO-NAs on a nanowire-like precursor by digital mechanoelectrospinning direct-writing (MES-Writing) technology[29,30], together with a subsequent hydrothermal synthesis and photoreduction reaction. Firstly, the digital MES-Writing technology was adopted to deposited large-scale aligned electrohydrodynamic nanowire template with high-density ZnO seed. The template can be fabricated in large-area substrate, and the diameter of nanowires is from 200 nm to 20 μm. The nanowire-diameter and nanowire-gap could be controlled digitally with arbitrary value. Secondly, these samples were put into oven with 200 °C for 2 hours, to form ZnAc/PEO nanoscale crystal nucleus. Thirdly, the hydrothermal synthesis method was utilized to selectively grow ZnO-NAs on the printed precursor pattern. The sample exhibits aligned parallel array and brush-like morphology of ZnO-NAs. The density of ZnO nanorods is determined by the seeds, the shape of ZnO nanorods results from the growth time of hydrothermal method, and the layout of ZnO nanorods depends on the aligned nanowires. It can be seen that uniform nanorods with diameters of ~400 nm and length of dozens of micrometers have been fabricated. Finally, Ag nanoparticles (Ag-NPs) are photoreduced on the surfaces of ZnO nanorods to form Ag/ZnO-NAs. It is worth mentioning that the morphology of the nanorod arrays remain the same even if the surface of ZnO nanorods are grown of Ag nanoparticles. The high-magnification field emission scanning electron microscopy (FESEM) images illustrate that the Ag-NPs with less than 50 nm in size are randomly and uniformly distributed on the surface of ZnO nanorods.

Figure 1b schematically and experimentally illustrates I) the compact ZnO nanorod arrays (ZnO-NAs) growing on film-like precursor, II) hybrid ZnO-NAs on ribbon-like precursor, and III) brush-like ZnO-NAs on nanowire-like precursor, from oblique view, front view and top view, respectively. For comparison, the ZnO NAs grown on film-like and ribbon-like precursors, respectively, are prepared with the same procedure. As shown in Fig. 1b (I and II), the ZnO nanorods on film-like precursor and the middle part of ribbon-like precursor crowd together, while the ZnO nanorods at edges of ribbon are interdigitated between adjacent parallel arrays[31]. The brush-like 3D h-Ag/ZnO-NAs compose of uniform nanoparticles, vertical nanorods and aligned nanowires. Obviously, the resolution and gap of deposited lines determine the exposure area with target gas molecules and reduced Ag nanoparticles (Ag-NPs). Therefore, more area of the brush-like ZnO-NAs on nanowire-like precursor can be exposed to target gas molecules so that the change in conductance of brush-like nanostructures will be greater. Figure 1b (III) shows the samples exhibit aligned parallel arrays and brush-like morphology of ZnO-NAs. The brush-like morphology contributes to Ag-NPs grown controllably on the surface of ZnO nanorods, and is chosen to form h-Ag/ZnO-NAs of nanoparticles(Ag)-on-nanorods(ZnO)-on-nanowires(precursor). Meanwhile high-density ZnO-NAs prevent Ag-NPs from growing on the surface of ZnO nanorods, and prevent the Ag/ZnO nanorods from contacting with gas. When brush-like Ag/ZnO-NAs are exposed to target gas, the change of conductance will be greater.

Morphologies and Structures. Structure and component of Ag/ZnO-NAs samples were confirmed by X-ray diffraction (XRD) and Transmission electron microscope (TEM). Typical XRD analysis of various Ag/ZnO samples are shown in Fig. 2, where samples photoreduced for 10 min, 20 min, 30 min, 40 min are marked as Ag/ZnO-10, Ag/ZnO-20, Ag/ZnO-30 and Ag/ZnO-40, respectively. The recorded diffraction patterns can be indexed into two groups: ZnO crystal and Ag^+. There are six well defined diffraction peaks (marked as "◆") at $2\theta = 31.88°$, 34.41°, 36.26°, 47.52°, 56.56° and 62.9° in all diffraction patterns, which correspond to (100), (002), (101), (102), (110) and (103) planes of ZnO crystal. This is the typical hexagonal wurtzite phase of ZnO. The lattice constants of ZnO are $a = 3.2498$ Å and $c = 5.2066$ Å (JCPDS card no. 36–1451). (002) peak has the maximum intensity, indicating that c-axis [0001] is the growth direction of ZnO nanorods. The other observed characteristic diffraction peaks of 38.2°, 44.4° and 64.6° (marked as "▼") match well with the (111), (200) and (220) peaks of Ag with the face-centered cubic (FCC) structure (JCPDS card no. 04–0783) with the lattice constant of $a = 4.0862$ Å, which proves that Ag^+ is photoreduced successfully. Additionally, there exist no characteristic peaks corresponding to other impurities, e.g. AgO and Ag_2O etc.

The XRD analysis shows the successful preparation of a binary phase consisting of wurtzite ZnO and FCC Ag in the samples. In addition, every ZnO diffraction peak has no notable shift for ZnO/Ag composites compared with pure ZnO samples. It indicates well crystal structure of the as-synthesized Ag/ZnO-NAs that Ag neither changes the intrinsic properties of ZnO nanocrystal nor incorporates into the lattice of ZnO. The expansion or

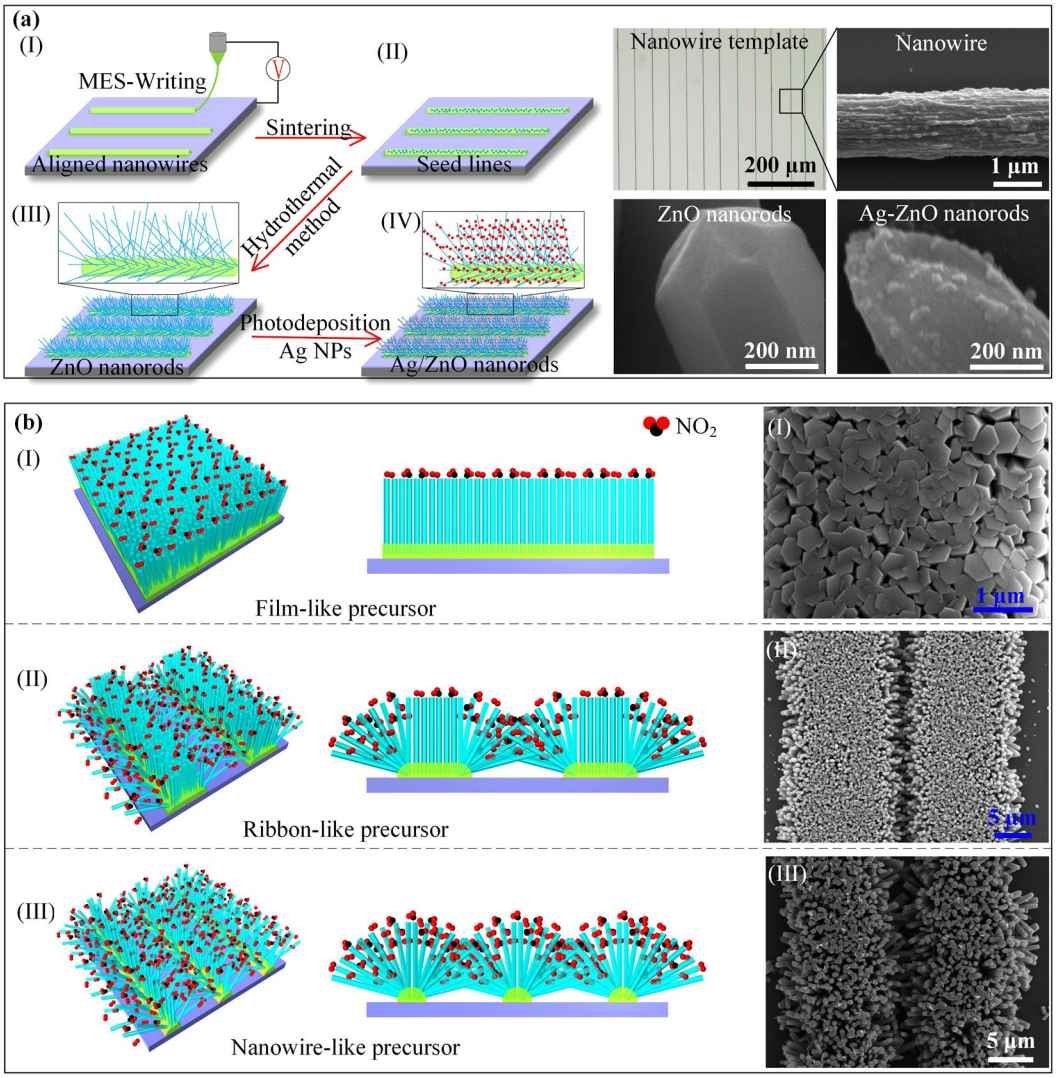

Figure 1. (**a**) The process steps of fabrication of Ag-ZnO NAs, and the optical images of nanowire template, FESEM image of nanowire, and FESEM images of ZnO nanorods and Ag-ZnO nanorods. (**b**) The schematic oblique and sectional views of NO_2 absorption of ZnO nanorod arrays from (I) film-like, (II) ribbon-like, and (III) nanowire-like precursors, respectively, and FESEM images of various ZnO-NAs grown on film-like, ribbon-like and nanowire-like seed layers, respectively.

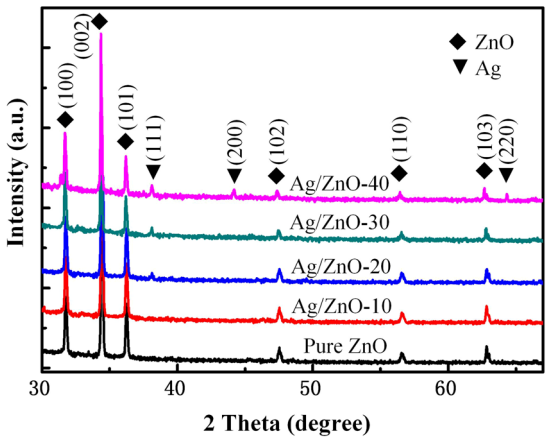

Figure 2. The XRD of samples of pure ZnO, Ag/ZnO-10, Ag/ZnO-20, Ag/ZnO-30 and Ag/ZnO-40.

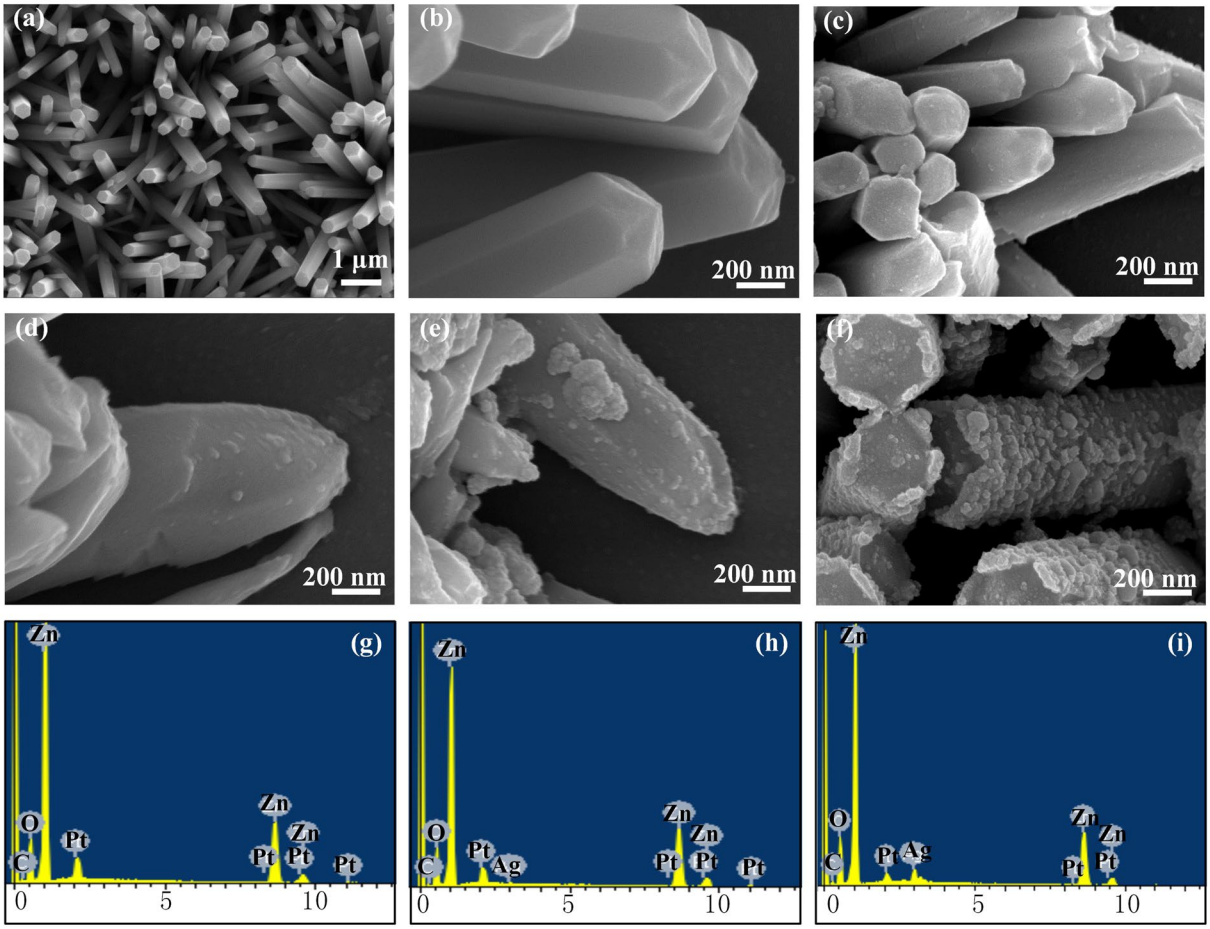

Figure 3. The FESEM images of (**a**,**b**) pure ZnO nanorods, (**c**) Ag/ZnO-10, (**d**) Ag/ZnO-20, (**e**) Ag/ZnO-30 and (**f**) Ag/ZnO-40. The EDXS spectra of (**g**) pure ZnO, (**h**) Ag/ZnO-30 and (**i**) Ag/ZnO-40.

shrinkage of ZnO lattice for Ag/ZnO nanocrystals should be negligible. By comparing peaks of ZnO and Ag, it is found that the peaks intensity of ZnO are gradually decreased and that of Ag nanoparticle are evidently increased evidently, with increasing the photoreduction time of Ag^+.

Figure 3 shows the FESEM images and energy dispersive X-ray spectrum (EDXS) spectrums of the obtained samples. The density of Ag-NPs on ZnO nanorods is determined by the photoreduction time, and the large cover area benefits from the specific area of brush-like structures. The comparison between ZnO nanorods and Ag-ZnO nanorods can be observed from the FESEM images. The size of Ag-NPs keeps almost constant when the photoreduction time is less than 30 min, but sharply increases when the photoreduction time reaches 40 min, and some of Ag-NPs aggregate into agglomerates (Fig. 3f). The gap between nanowires plays another critical role in the improvement of specific area. The length of ZnO nanorods determines the optimal gap between lines, and the optimal gap is ~20 μm. The morphologies of the Ag/ZnO nanorods with various Ag content are shown in Fig. 3(c,d,e,f). The surfaces of Ag/ZnO nanorods are rough compared to that of pure ZnO nanorods. Additionally, the quantity of the Ag-NPs monotonously increases with the photoreduction time, which agrees with XRD analysis of Fig. 2.

The Ag-NPs can grow uniformly on both top and lateral surfaces of ZnO nanorods, which is attributed to several reasons. Free electron, Ag^+ and UV light are the necessary conditions for the formation of Ag-NPs. When the surface of ZnO-NAs are irradiated with UV light (400 W) many electrons will be accumulated on both top and lateral surfaces of ZnO nanorods. The brush-like ZnO-NAs, on one hand, is favorable for the diffusion of Ag^+ on the surfaces of ZnO nanorods. On the other hand, it plays a role as reflector in light trapping structure, which reflects the UV light to the root of ZnO nanorod. Thus, Ag-NPs can be easily formed on both top and lateral surface of ZnO nanorods.

TEM/HAADF-STEM/HRTEM images further reveal the structure of Ag/ZnO samples. As shown in Fig. 4c–f, the TEM images show that Ag/ZnO-30 and Ag/ZnO-40 are covered with dispersed Ag-NPs (highlighted by red dash-line quadrangles) with an average diameter of dozens of nanometers in size, while there is no attachment for pure ZnO nanorods (Fig. 4a,b). EDXS image shows that except the C and Pt elements arise from sprayed carbon and Pt before scanning, the sample only contains the element of Zn, O, and Ag. In addition, the Ag peak intensity of Ag/ZnO-40 (Fig. 3i) is higher than that of Ag/ZnO-30 (Fig. 3h). It indicates that Ag-NPs grow well on the surface of ZnO nanorods. There are no other element peaks, which is consistent with the analysis result of XRD.

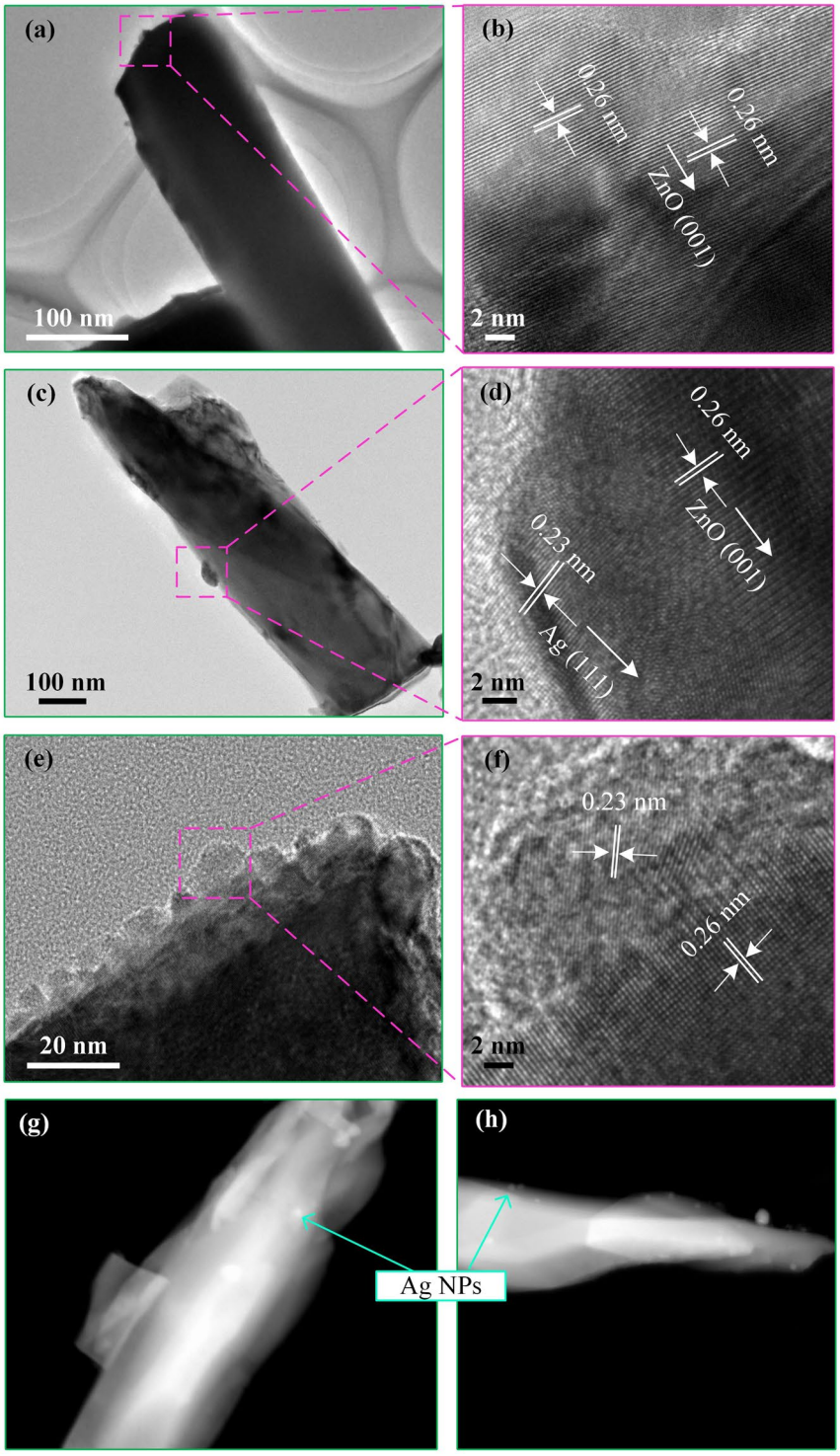

Figure 4. TEM images of (**a**,**b**) pure ZnO and (**c**,**d**) Ag/ZnO-30, (**e**,**f**) Ag/ZnO-40 nanostructures, and HAADF-STEM images of (**g**) Ag/ZnO-30 and (**h**) Ag/ZnO-40.

The bright spots in cyan solid line circles in the HAADF-STEM images reveal that the Ag-NPs are distributed along the ZnO nanorods (Fig. 4g and h). The quantity of Ag-NPs in Fig. 4e is larger than that in Fig. 4c due to the increase of Ag^+ photoreduction time. HRTEM images (Fig. 4b,d and f) show that the lattice fringes of ZnO and Ag. The lattice fringes of pure ZnO nanorods are revealed clearly in Fig. 4b. The measured lattice space is 0.26 nm, which is the space of the (001) plane, revealing that the growth direction of ZnO nanorods is [0001]. The lattice fringes with inter planar spacing of 0.23 nm are corresponding to the (111) plane of FCC Ag (Fig. 4d,f). So ZnO-NAs are successfully modified by Ag NPs, which is in good agreement with the results of XRD.

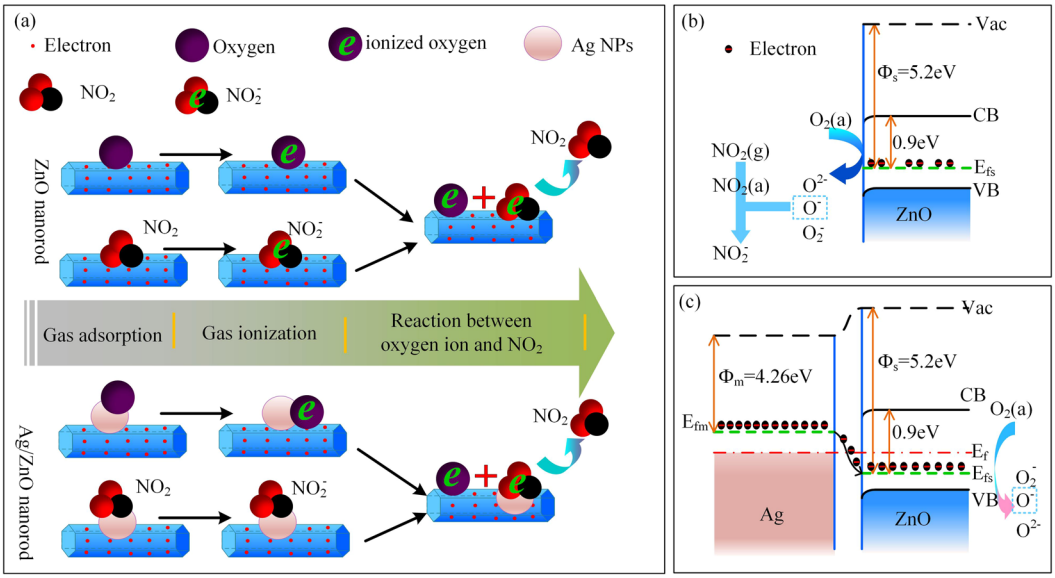

Figure 5. The chemical sensitization mechanism (**a**) of catalytic property for Ag-NPs on ZnO nanorods. The energy band structures of pure ZnO (**b**) and the Fermi energy level equilibrium of Ag-ZnO junction (**c**).

Sensing mechanism. The main carriers are free electrons of the conduction band (C.B.) for n-type ZnO, and the main charge acceptor on ZnO surface is oxygen molecule. Thus the free electrons in C.B. of ZnO ionized the adsorbed oxygen species, and ionized oxygen species such as O_2^-, O^- and O^{2-} were formed[32]. Oxygen adsorption reactions highly depend on working temperature, and the stable oxygen ions are O_2^-, O^- and O^{2-} at below 100 °C, within 100–300 °C and above 300 °C operating temperature, respectively[33]. The lower concentration of free electrons in C.B. of ZnO increases the resistance[34]. When NO_2 gas molecules are adsorbed on the surface of ZnO nanorods, it attracts the free electrons from the C.B. of ZnO. NO_2 molecules have higher electrophilic property, and they can capture the electronics from ZnO and react with the oxygen ions to decrease the electron concentration. The surface depletion region of ZnO nanorods is further widen, so the resistance further increases. All the involved reactions are described in detail in Supporting Information. When NO_2 concentration increases, more electrons will be involved in above reactions. The resistance of ZnO samples is modulated by the adsorption and desorption of gas molecules.

The Ag-NPs is attribute to gas sensing performance based on catalytic surface reactivity of Ag-NPs and the Schottky junctions formed on the interface between Ag and ZnO[35]. Figure 5a shows the schematic diagram of catalytic property for Ag/ZnO sensor. The Ag-NPs can tune carrier concentration in ZnO nanorods. The oxygen molecule is adsorbed on Ag catalyst preferentially and then spill over to ZnO matrix. The NO_2 molecules are adsorbed onto the surface of Ag-NPs and then react with oxygen species and electrons. The electrons captured by adsorbed oxygen ions are delivered, leading to an enhanced sensing response. The effect of Schottky junction refers to the electron exchange between Ag and ZnO, enhancing the separation of charge carriers and lifetime of electrons[36]. For pure ZnO sensor, the absorbed oxygen is ionized via combining with the spill-over electrons of the Fermi energy level (E_{fs}) in ZnO (Fig. 5b). The work function (Φ_s) of ZnO (5.2 eV) is larger than that of silver ($\Phi_m = 4.26$ eV), and the E_{fs} of ZnO is lower than the Fermi energy level of Ag (E_{fm}). When Ag-NPs are adopted, partial electrons migrate from Ag to ZnO until the two systems attain equilibrium and the new uniform Fermi energy level is formed (E_f), as described in Fig. 5c. When $E_f > E_{fs}$, more oxygen will be absorbed. Above two mechanisms both could modulate the sensing reactions between target gas and oxygen species to realize better sensing performance.

The effect of Ag-NPs on gas sensing performance of ZnO-NAs. The chemical sensing performances of these samples were then investigated. The resistance (R) of these samples was tested in clean and dry air to get the baseline resistance Ra. R increases (decreases) to a maximum (minimum) value Rg when the sensor is placed in different concentrations of target gas. Sensor response S is defined as $S = (Rg - Ra)/Ra$ for oxidizing gas and $S = (Ra - Rg)/Ra$ for reducing gas. The responses of ZnO and Ag/ZnO samples to different kinds of gases are shown in Fig. 6. The Ag/ZnO-based sensors show much higher response to NO_2 gases than other gases such as SO_2, methane, CO, ethanol, methanol, NH_3, H_2, and formaldehyde at the working temperature of 225 °C. The highest response is 54.0 to 10 ppm NO_2 but is less than 1.2 toward other gases even at higher concentration. So the samples show highly selective sensing properties for NO_2 gas, which can distinguish the NO_2 gas among the mixture gases. It is consistent with the results obtained by other authors[37].

Figure 7a shows dynamic responses of ZnO and Ag/ZnO samples to NO_2 at various concentrations (from 1 to 50 ppm) at 225 °C. Ag/ZnO samples are n-type gas sensors like pure ZnO, whose resistances increase to maximum value after injection of oxidizing NO_2 gas into the testing chamber. The response to NO_2 is rapid, steady and reproducible when the samples are in NO_2 atmosphere. The responses of pure ZnO and Ag/ZnO sensors both

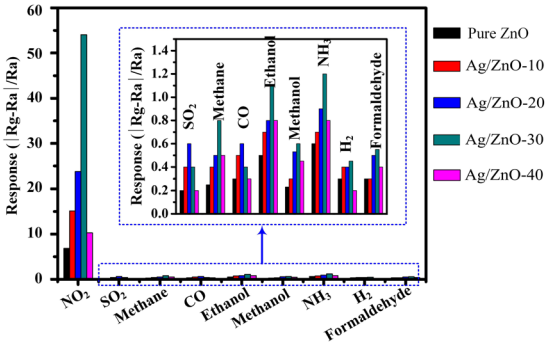

Figure 6. Responses of pure ZnO and Ag-ZnO samples toward NO_2(10 ppm), SO_2(50 ppm), methane (50 ppm), CO(10 ppm), ethanol(10 ppm), methanol(10 ppm), NH_3(50 ppm), H_2(10 ppm), and formaldehyde (10 ppm) at the working temperature of 225 °C.

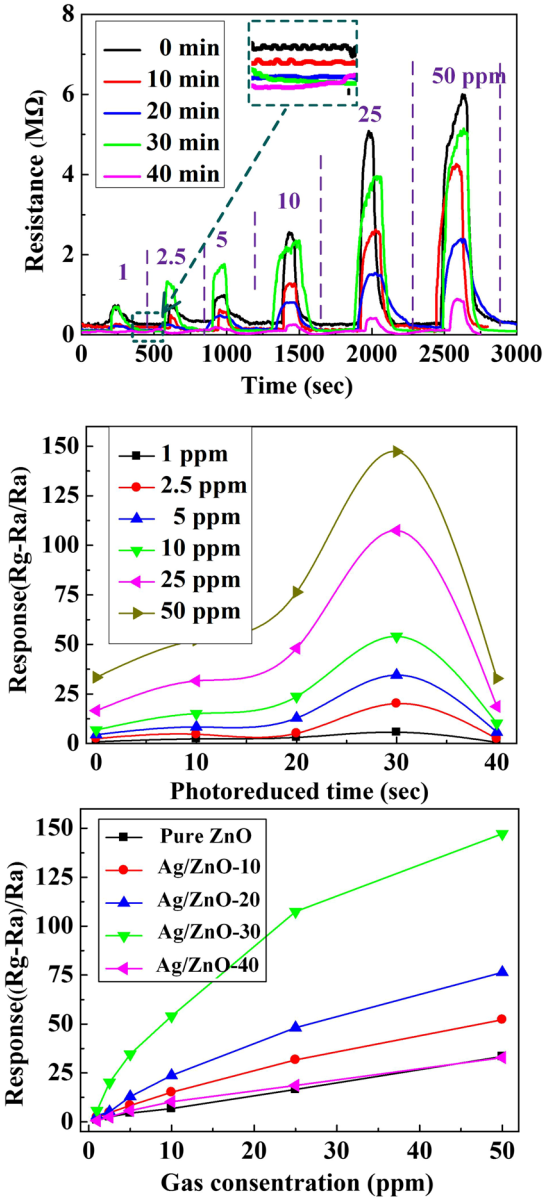

Figure 7. (**a**) The dynamic responses of pure ZnO and Ag-ZnO samples in different NO_2 concentrations. The inset of figure (**a**) is the baseline of samples. Response (**b**,**c**) of the pure ZnO and Ag-ZnO sensors to different concentrations of NO_2 at the same working temperature.

increase with NO_2 concentration increasing. The resistances can recover to the original baseline level completely with removing NO_2 for all samples. The morphologies of ZnO-NAs have large advantage for gas sensing. The brush-like morphology of ZnO-NAs is more beneficial to gas transmission and adsorption than that of vertically compact ZnO-NAs[38]. the interdigitated nanorods between the adjacent arrays contribute to gas response. Moreover, most junctions between nanorods are point junctions rather than cross junctions and block junctions, which is beneficial for gas sensing performance[39]. ZnO nanorods are oriented in [0001], which have the best gas sensing activity[40]. Because the [0001] plane terminated with Zn^{2+} ion is concerned, which is able to seize atmosphere O_2 through physical/chemical absorption.

Ag-NPs release free electrons which increase carrier concentration and conductance of ZnO. So the baseline resistance *Ra* of sensors is decreased when the photoreduction time of Ag^+ ions increase (the inset of Fig. 7a). The *Ra* of pure ZnO, Ag/ZnO-10, Ag/ZnO-20, Ag/ZnO-30 and Ag/ZnO-40 are 0.17 MΩ, 0.1 MΩ, 0.04 MΩ, 0.035 MΩ and 0.016 MΩ, respectively. Gas response increases with the photoreduction time (the Ag content) up to 30 min and then decreases sharply for Ag/ZnO-40 sample (Fig. 7b). It indicates that NO_2 sensing property of ZnO nanorods sensor can be enhanced by Ag-NPs modification, and reach the highest response value at the photoreduction time of 30 min. When Ag-NPs exceed the optimal content, they reversely behave as recombination centers of charge carriers[41], which is caused by the electrostatic attraction of charged Ag (negatively) and charged holes (positively)[42]. When the concentrations of NO_2 are 1 ppm, 2.5 ppm, 5 ppm, 10 ppm, 25 ppm, 50 ppm, the responses of pure ZnO sample are 0.96, 2.56, 4.47, 6.84, 16.59, 33.44, and the responses of Ag/ZnO-30 are 5.77, 20.16, 34.53, 54.07, 107.43, 147.19, respectively. The responses of Ag/ZnO-30 are at least two times higher than that of pure ZnO-NAs for the same concentration of NO_2. Meanwhile, the response time (less than 120 s) and recovery time (less than 150 s) for all h-Ag/ZnO-NAs gas sensor at every test concentrations of NO_2 are of the order of mins. And the detection limits can be achieved 1 ppm or less.

In addition, gas sensing performance can be described by the tangents of response curves. The tangent of Ag/ZnO-30 sample response curve (Fig. 7c) is larger than that of other samples at various gas concentrations. Gas response decreases sharply for Ag/ZnO-40 sensors, since too much surface of ZnO is occupied by Ag-NPs, which influences the adsorption of oxygen and NO_2 gas molecular. So Ag/ZnO-30 gas sensor has the best sensing property. It indicates that the gas responses increase when NO_2 concentration increases (Fig. 7c). There is an approximately linear increase relationship between the response and NO_2 concentration for pure ZnO, Ag/ZnO-10 and Ag/ZnO-20 samples. Specifically, the gas sensing performance increases with increasing photoreduction time of Ag ions from 10 to 30 min. However, further increasing photoreduction time to 40 min induces excessive Ag-NPs, leading to the decrease of gas sensing performance. The influence of Ag-NPs on the gas response performance of Ag/ZnO samples is attribute to the concurrence of two parallel phenomena. 1) Ag-NPs promote oxygen adsorption/dissociation, which consists in catalytic activation of oxygen dissociation on the semiconductor to enhance the surface reactivity. 2) The electronic effect consisting in electron of Ag injected into the C.B. of ZnO can be traced back to the formation of Schottky junctions at the Ag-ZnO interface. These studies hint the potential application of gas sensor based on Ag/ZnO-NAs in monitoring NO_2.

In summary, aligned h-Ag/ZnO-NAs of nanoparticles-on-nanorods-on-nanowires were fabricated by a multiscale synthesis method via a MES-Writing technology, together with a subsequent hydrothermal growth and photoreduction. Such aligned h-Ag/ZnO-NAs exhibit significant enhancement in gas sensing performance, and this is ascribed to the higher specific area, surface reactivity, and the Schottky junctions at the interface between Ag and ZnO. The fabrication processes shows great influence on the sensing performance as well. And the proposed synthesis method can be used to prepare aligned h-Ag/ZnO-NAs in a digital, large-area and cost-effective manner, which would be a valuable technique for the fabrication of advanced sensing devices.

Materials and Methods

Materials. PEO (Polyethylene oxide) is purchased from Aldrich. $Zn(CH_3COO)_2{\cdot}2H_2O$ (ZnAc), $Zn(NO_3)_2{\cdot}6H_2O$, hexamethylenetetramine (HMTA) and silver nitrate($AgNO_3$) are purchased from Sinopharm Chemical Reagent Co., Ltd.

Synthesis of patterned ZnO nanorod arrays. The aligned nanowires with tunable diameter and distance were directly deposited on substrate via MES-Writing. ZnO-NAs grew on the nanowires by a selective hydrothermal synthesis method. In a typical procedure, an aqueous solution of PEO (600,000, 6 wt%) and ZnAc (0.05 M) was printed by MES-Writing on alumina substrate with Ag interdigital electrodes (IDT). Then the substrate was sintered at 200 °C for 2 hours (h), and a ZnAc seed layer was formed. The seeded substrate was immersed into a Teflon-lined stainless steel autoclave filled with mixed aqueous solution containing 0.05 M $Zn(NO_3)$ and 0.05 M HMTA. ZnO-NAs grow on nanowires at 90 °C. After 12 h of hydrothermal reaction, the substrate was taken out of the mixed aqueous solution, washed with deionized water, then dried at 60 °C.

Synthesis of Ag/ZnO-NAs. The Ag/ZnO-NAs were prepared by photodeposition method. The distribution and density of ZnO-NAs with 20 μm distance between nanowires were suitable for Ag-NPs deposition and gas sensitive reaction. $AgNO_3$ was dissolved in the mixed solvent of deionized water and absolute ethyl alcohol to form 0.01 M $AgNO_3$ solution by magnetic stirring for 0.5 h in dark. The ratio of deionized water to absolute ethyl alcohol was 4:1. The ZnO-NAs were preirradiated with 400 W UV light (wavelength: 365 nm) for 1 h to enhance their hydrophility and then were immersed into 100 mL 0.01 M $AgNO_3$ solution in a quartz flask for 1 h to make sure that Ag^+ ions adsorbed onto ZnO surfaces completely. The above ZnO-NAs were put into another 0.01 M $AgNO_3$ solution in a closed container which was filled with flowing pure N_2 to prevent oxidation. Ag^+ ions were photoreduced by irradiation of the sample and $AgNO_3$ solution with UV light. The Ag-NPs were photodeposited onto the surfaces of ZnO nanorods. The Ag content is controlled through the UV irradiation time. Finally, these samples were rinsed with deionized water to remove the residual Ag^+. The energy of photon ($h\nu$) of UV light

(3.397 eV) is larger than the band gap of ZnO ($Eg = 3.37$ eV), leading to the generation of electron-hole pairs. Ethanol acts as the hole scavenger to consume the photo-induced holes, leaving the unpaired electrons on ZnO surface[43]. The photogenerated holes (h^+) in the valence band are consumed to oxidize C_2H_5OH to produce ethoxy radicals $C_2H_4OH\bullet$. Meanwhile the accumulated electrons (e^-) in the C.B. contribute to reduce Ag^+ to form Ag-NPs *in situ* on ZnO nanorods.

Characterization and Measurement of Gas Sensor. The microstructure of pure ZnO and Ag/ZnO-NAs were characterized by TEM (JEM-2100F STEM/EDXS, JEOL) and FESEM (Sirion200, FEI). The morphologies and crystal planes of the samples were investigated by FESEM at 20 kV sputtering a thin film of Pt and TEM including high-resolution transmission electron microscope (HRTEM) and High-angle annular dark field scanning transmission electron microscopy (HAADF-STEM). The crystalline structure, nanorod growth direction and composition of the samples were analyzed by an XRD (Philips X'Pert PRO diffractometer) with Cu-Kα radiation ($\lambda = 1.5418$ Å). The gas responses of ZnO sensors were measured using a homemade test system. The gas dilution system is used for gas sensing measurement. A resistive heater is utilized for the control of operating temperature. The gas sensors are fixed in the chamber, and Ag interdigital electrodes connect with two probes. 4.096 V (DC) power is supplied to the signal resistor R_0 and sensor. The voltage across R_0 is continuously recorded as V_0, when a ZnO sample is alternately exposure to air and target gas atmosphere at a certain temperature. The resistance of the sensor R can be calculated obtained by Ohm's law.

References

1. Wang, X. *et al*. Highly sensitive, temperature-dependent gas sensor based on hierarchical ZnO nanorod arrays. *Journal of Materials Chemistry C* **3**, 11397–11405 (2015).
2. Shi, J. P. & Harrison, R. M. Regression modelling of hourly NOx and NO_2 concentrations in urban air in London. *Atmospheric Environment* **31**, 4081–4094 (1997).
3. Vayssieres, L. Growth of arrayed nanorods and nanowires of ZnO from aqueous solutions. *Advanced Materials* **15**, 464–466 (2003).
4. Uddin, A. S. M. I. & Chung, G.-S. Synthesis of Highly Stable Silver-Loaded Vertical ZnO Nanowires Array and its Acetylene Sensing Properties. *Surface Review and Letters* **23**, 1550087 (2016).
5. Suo, C. *et al*. Ag-decorated ZnO nanorods prepared by photochemical deposition and their high selectivity to ethanol using conducting oxide electrodes. *RSC Advances* **5**, 92107–92113 (2015).
6. Iftekhar Uddin, A. S. M., Phan, D.-T. & Chung, G.-S. Low temperature acetylene gas sensor based on Ag nanoparticles-loaded ZnO-reduced graphene oxide hybrid. *Sensors and Actuators B: Chemical* **207**, Part A, 362–369 (2015).
7. Oleiwi, H. F. *et al*. Two-dimensional CdS intercalated ZnO nanorods: a concise study on interfacial band structure modification. *RSC Advances* **6**, 52395–52402 (2016).
8. Tan, S. T. *et al*. Laser stimulated electrooptics in the Ag–ZnO nanorods. *Physica E: Low-dimensional Systems and Nanostructures* **61**, 23–27 (2014).
9. Tan, S. T. *et al*. Ag–ZnO nanoreactor grown on FTO substrate exhibiting high heterogeneous photocatalytic efficiency. *ACS combinatorial science* **16**, 314–320 (2014).
10. Vuong, N. M., Chinh, N. D., Huy, B. T. & Lee, Y.-I. CuO-Decorated ZnO Hierarchical Nanostructures as Efficient and Established Sensing Materials for H_2S Gas Sensors. *Sci Rep* **6**, 26736 (2016).
11. Yang, T. H. *et al*. High Density Unaggregated Au Nanoparticles on ZnO Nanorod Arrays Function as Efficient and Recyclable Photocatalysts for Environmental Purification. *Small* **9**, 3169–3182 (2013).
12. Quentin, S. *et al*. Ag/ZnO nanomaterials as high performance sensors for flammable and toxic gases. *Nanotechnology* **23**, 025502 (2012).
13. Simon, Q. *et al*. Plasma-assisted synthesis of Ag/ZnO nanocomposites: First example of photo-induced H_2 production and sensing. *Int J Hydrogen Energy* **36**, 15527–15537 (2011).
14. Dinesh, V., Sukhananazerin, A. & Biji, P. An emphatic study on role of spill-over sensitization and surface defects on NO_2 gas sensor properties of ultralong ZnO@ Au heterojunction NRs. *J Alloys Compd* **712**, 811–821 (2017).
15. Bekermann, D. *et al*. Co_3O_4/ZnO nanocomposites: from plasma synthesis to gas sensing applications. *ACS Appl Mat Interfaces* **4**, 928–934 (2012).
16. Simon, Q. *et al*. CuO/ZnO Nanocomposite Gas Sensors Developed by a Plasma-Assisted Route. *ChemPhysChem* **13**, 2342–2348 (2012).
17. Kim, H. W. *et al*. Synthesis of zinc oxide semiconductors-graphene nanocomposites by microwave irradiation for application to gas sensors. *Sens Actuators, B* **249**, 590–601 (2017).
18. Her, Y.-C., Yeh, B.-Y. & Huang, S.-L. Vapor–solid growth of p-Te/n-SnO_2 hierarchical heterostructures and their enhanced room-temperature gas sensing properties. *ACS applied materials & interfaces* **6**, 9150–9159 (2014).
19. Lou, Z., Li, F., Deng, J., Wang, L. & Zhang, T. Branch-like hierarchical heterostructure (α-Fe_2O_3/TiO_2): a novel sensing material for trimethylamine gas sensor. *ACS applied materials & interfaces* **5**, 12310–12316 (2013).
20. Cheng, C. *et al*. Hierarchical assembly of ZnO nanostructures on SnO_2 backbone nanowires: low-temperature hydrothermal preparation and optical properties. *ACS nano* **3**, 3069–3076 (2009).
21. Wang, L. *et al*. Construction of 1D SnO_2-coated ZnO nanowire heterojunction for their improved n-butylamine sensing performances. *Sci Rep* **6**, 35079 (2016).
22. Choi, H.-J., Choi, S.-J., Choo, S., Kim, I.-D. & Lee, H. Hierarchical ZnO Nanowires-loaded Sb-doped SnO_2-ZnO Micrograting Pattern via Direct Imprinting-assisted Hydrothermal Growth and Its Selective Detection of Acetone Molecules. *Sci Rep* **6**, 18731 (2016).
23. Yadian, B. *et al*. Towards Perfectly Ordered Novel ZnO/Si Nano-Heterojunction Arrays. *Small* **10**, 344–348 (2014).
24. Zhou, C. *et al*. Ultrasensitive non-enzymatic glucose sensor based on three-dimensional network of ZnO-CuO hierarchical nanocomposites by electrospinning. *Sci Rep* **4**, 7382 (2014).
25. Peeters, D. *et al*. Au/ε-Fe_2O_3 nanocomposites as selective NO_2 gas sensors. *J Phys Chem C* **118**, 11813–11819 (2014).
26. Liu, X., Zhang, J., Guo, X., Wu, S. & Wang, S. Amino acid-assisted one-pot assembly of Au, Pt nanoparticles onto one-dimensional ZnO microrods. *Nanoscale* **2**, 1178–1184 (2010).
27. Zhao, Y. Y. *et al*. Pt/ZnO nanoarray nanogenerator as self-powered active gas sensor with linear ethanol sensing at room temperature. *Nanotechnology* **25**, 115502 (2014).
28. Zhang, Y. *et al*. Self-assemblies of Pd nanoparticles on the surfaces of single crystal ZnO nanowires for chemical sensors with enhanced performances. *Journal of Materials Chemistry* **19**, 4701–4706 (2009).
29. Huang, Y. A. *et al*. Electrohydrodynamic direct-writing. *Nanoscale* **5**, 12007–12017 (2013).
30. Onses, M. S., Sutanto, E., Ferreira, P. M., Alleyne, A. G. & Rogers, J. A. Mechanisms, Capabilities, and Applications of High-Resolution Electrohydrodynamic Jet Printing. *Small* **11**, 4237–4266 (2015).

31. Wang, X., Sun, F., Huang, Y., Duan, Y. & Yin, Z. A patterned ZnO nanorod array/gas sensor fabricated by mechanoelectrospinning-assisted selective growth. *Chemical Communications* **51**, 3117–3120 (2015).
32. Şahin, Y. *et al*. Electrical conduction and NO_2 gas sensing properties of ZnO nanorods. *Applied Surface Science* **303**, 90–96 (2014).
33. Ghimbeu, C. M., Schoonman, J., Lumbreras, M. & Siadat, M. Electrostatic spray deposited zinc oxide films for gas sensor applications. *Applied Surface Science* **253**, 7483–7489 (2007).
34. Shi, L. *et al*. Highly Sensitive ZnO Nanorod- and Nanoprism-Based NO_2 Gas Sensors: Size and Shape Control Using a Continuous Hydrothermal Pilot Plant. *Langmuir* **29**, 10603–10609 (2013).
35. Basu, S. & Basu, P. Nanocrystalline metal oxides for methane sensors: role of noble metals. *Journal of Sensors* **29**, 861968 1–20 (2009).
36. Barreca, D. *et al*. Novel synthesis and gas sensing performances of CuO–TiO_2 nanocomposites functionalized with Au nanoparticles. *The Journal of Physical Chemistry C* **115**, 10510–10517 (2011).
37. Jiao, M. *et al*. On-chip hydrothermal growth of ZnO nanorods at low temperature for highly selective NO_2 gas sensor. *Materials Letters* **169**, 231–235 (2016).
38. Ahn, M.-W. *et al*. Gas Sensing properties of Defect-Controlled ZnO-Nanowire Gas Sensor. *Applied Physics Letters* **93**, 263103 (2008).
39. Lee, H. U. *et al*. ZnO nanobarbed fibers: Fabrication, sensing NO_2 gas, and their sensing mechanism. *Applied Physics Letters* **98**, 193114 (2011).
40. Han, X.-G. *et al*. Controlling Morphologies and Tuning the Related Properties of Nano/Microstructured ZnO Crystallites. *The Journal of Physical Chemistry C* **113**, 584–589 (2009).
41. Lin, S.-L., Hsu, K.-C., Hsu, C.-H. & Chen, D.-H. Hydrogen treatment-improved uniform deposition of Ag nanoparticles on ZnO nanorod arrays and their visible-light photocatalytic and surface-enhanced Raman scattering properties. *Nanoscale Research Letters* **8**, 1–9 (2013).
42. Sun, F., Qiao, X., Tan, F., Wang, W. & Qiu, X. One-step microwave synthesis of Ag/ZnO nanocomposites with enhanced photocatalytic performance. *Journal of Materials Science* **47**, 7262–7268 (2012).
43. Liu, Y., Wei, S. & Gao, W. Ag/ZnO heterostructures and their photocatalytic activity under visible light: Effect of reducing medium. *Journal of Hazardous Materials* **287**, 59–68 (2015).

Acknowledgements

This work was supported by the National Natural Science Foundation of China (51635007, 91323303) and National Key R&D Program (2016YFB0401105). The experimental support of Comprehensive Experiment Center for Advanced Manufacturing and Equipment Technology is also acknowledged.

Author Contributions

Z.P. Yin, X.M. Wang, and Y.A. Huang designed the experiments and wrote the manuscript. Z.P. Yin and X.M. Wang performed the direct-writing experiments. F.Z. Sun, X.H. Tong, C. Zhu, and Q.Y. Lv performed the gas sensing experiments. D. Ye, S. Wang and W. Luo analyzed the data, and discussed the results. All authors reviewed the manuscript.

Additional Information

Supplementary information accompanies this paper at https://doi.org/10.1038/s41598-017-12553-7.

Competing Interests: The authors declare that they have no competing interests.

Publisher's note: Springer Nature remains neutral with regard to jurisdictional claims in published maps and institutional affiliations.